CrystEngComm

Accepted Manuscript

ROYAL SOCIETY OF CHEMISTRY

www.rsc.org/crystengcomm

Growth and characterization of piezoelectric benzil single crystals and its application in microstrip patch antenna

Harsh Yadav [a], Nidhi Sinha [b] and Binay Kumar [a,*]

[a]Crystal Lab, Department of Physics & Astrophysics, University of Delhi, Delhi 110007, India

[b]Department of Physics & Electronics, SGTB Khalsa College, University of Delhi, Delhi 110007, India

Corresponding author: Dr. Binay Kumar; M: +91-9818168001; email: b3kumar69@yahoo.co.in

Abstract

Organic non linear optical single crystals of benzil have been grown by Czochralski (Cz) and slow-evaporation techniques. Crystal morphology was characterized by computing the growth rates of the planes which was found to be affected by solvent modification. Intermolecular interactions of the benzil crystal was explored by Hirshfeld surface and 2D fingerplot in a novel visual manner. A linear optical study was carried out by UV-Vis transmission spectrum in which Cz grown crystal was found to be more transparent with cut off wavelength at 406 nm. Photoluminescence emission spectrum was observed at green region with higher intensity in Cz grown crystal. The piezoelectric charge coefficients were found to be 4, 1, 6 and 3 pC/N along (100), (010), (001) and $(\bar{1}10)$ planes of the solution grown crystal. The study of Vicker's microhardness and volume of voids in the grown crystals confirmed that the Cz grown crystal has better mechanical strength. Patch antenna based on the substrate of Cz grown benzil crystal was simulated for resonant frequency at 12.6 GHz and fabricated which is suitable for piezoelectric, sensor and telecommunication applications.

Introduction

The linear and non-linear optical responses of the organic crystal are highly anisotropic in nature.[1] In most generalized principal of higher nonlinear optical (NLO) activity, electronic structure of the organic molecule are effectively coupled to electric field of the radiation with non-centrosymmetric space group and resonant technique are checked to magnify the optical response.[2] Distinguish optical properties of the organic molecules helps the technology for miniaturization and fast processing of the data.[3] High intensity laser radiation is needed to establish the non-linear relationship between the polarization and electric field. The different application range of the laser has been extended by using harmonic generators (NLO crystals) for highly sensitive characterization methods.[4] Low value of the dielectric constant in organic crystal helps in lowering the power consumption and decrease of the RC delay in microelectronics.[5]

Benzil is a good NLO molecular crystal and also possess first order improper ferroelectric transition at 83.5 K.[6] Single crystals of the benzil crystal was grown by different techniques like slow evaporation, Sankaranarayanan-Ramasamy method, Cz techniques, etc.[7-9] Benzil single crystal belongs to the non-centrosymmetric space group and exhibits both NLO and piezoelectric properties.[10] The organic ferroelectric semiconductor and NLO aspects of the benzil crystal makes it interesting for the design of the interface between optical and electrical communication network.[11] Glide dislocations was occurred in the undercooled melt growth of the benzil crystal due to its plastic nature near melting point.[12] For the growth of the dislocation-free benzil crystal, standard necking was not effective and growth behavior depends on the shape of solid-liquid interface.[13] K. Katoh et al. have reported that Burger vector c/3 is associated with the screw dislocation and defects is etched off from the crystal to use as a seed in the further growth.[13] It is reported that nonlinear optical properties of the benzil crystal is improved by metallic ion (Nd^{3+},

Cd^{2+}) dopants.[14] The critical behavior of the annealed and unannealed crystal of the benzil is reported in the literature by Brillouin scattering techniques.[15] Subhas Ch. Bera et al. have investigated the crystal spectrum of the benzil doped stilbene.[16] The flexible configuration of the benzil molecule probing the photochemical effect on the host environment of supramolecular solids is reported.[17] The change in photoluminescence and SHG as a result of *o*-Nitroaniline doping in benzil crystals have been reported.[18] However, piezoelectric property of the benzil crystal has not been reported so far which have been investigated in the present work. Piezoelectric response is directly affected by the π- π stacking of the benzil molecule in the crystal to polarize the H bond in the presence of electric field.[19] Benzil crystal belongs to the category of low dielectric constant material, which makes it applicable for microwave applications.[20] During crystal growth, additives affect the morphology by changing the growth rate of various planes of grown crystal.[21] Morphological studies of the benzil crystal were analyzed by modified Bravais-Friedel-Donnay-Harker (BFDH) law and its accuracy was checked with experimentally observed morphology.[22] Molecular surface of the benzil compound was computed on the basis of Hirshfeld surface analysis to understand the intermolecular interactions and hardness of the crystal was compared based on void volume estimation.[23-24] Patch antenna designed on the benzil single crystal substrate (with low dielectric constant 4.48) can be used in many wireless application such as Wi-Fi LAN, Bluetooth, pressure sensor, temperature sensor, crack propagation and shift in resonant frequency by dc biasing.[25-26] Moreover, the tunability is attained in this proposed antenna which is confirmed by the shift in resonant frequency on the application of dc voltage.[27] In addition, the common crystal geometry acts as an antenna and also as a piezoelectric energy harvesting device.[28] The grown crystals

were subjected to different characterizations such as single crystal XRD, UV-Vis transmission analysis, photoluminescence, hardness and dielectric studies.

Experimental

Crystal growth and characterization

The benzil crystals were grown by Czochralski as well as slow evaporation techniques. Saturated solution of the benzil in acetone was prepared to grow the benzil crystals by slow evaporation method. The solution grown benzil crystals are shown in Fig. 1(a, b). Fig. 1(c) shows the solution grown benzil crystal in the environment of acetone mixed with 0.5 M % of 5CB (4-Cyano-4'-pentylbiphenyl) nematic liquid crystal (LC) as an additive at RT. In the Cz method, a constant pulling and rotation rates of 2 mm/h and 20 r/min were used to grow the benzil crystal along (001) plane. The title compound was melted in 100 mm diameter aluminum crucible to grow the benzil single crystal. The dimensions of the grown crystal were 20 mm diameter and 20 mm cylindrical length (Figure 1 (d)). Single crystal XRD of the benzil crystal was taken using an Oxford Diffractometer (MoKα X-ray Source λ = 0.71073 Å). The UV–Vis transmittance spectrum was studied in the range 200–1100 nm by SHIMADZU UV-2501PC. PL emission spectrum was recorded by using Horiba Jobin Yvon Spectrophotometer. The Vicker's microhardness tester was used to measure the variation of hardness with respect to the indented load for a fixed dwell time of 10 second. Hirshfeld surfaces and voids in the crystal system were analysed using Crystal-Explorer 3.1 programme.[29] Dielectric studies were carried out by impedance analyzer (Agilent E 4980A) in the frequency range 1 kHz - 2 MHz at RT with applied DC voltage. The characteristic of the patch antenna was measured by vector network analyser (Agilent 8722ES). Piezoelectric analysis was carried out using Piezometer (PM 300 Piezotest) at a tapping frequency of 110 Hz with tapping force 0.25 N.

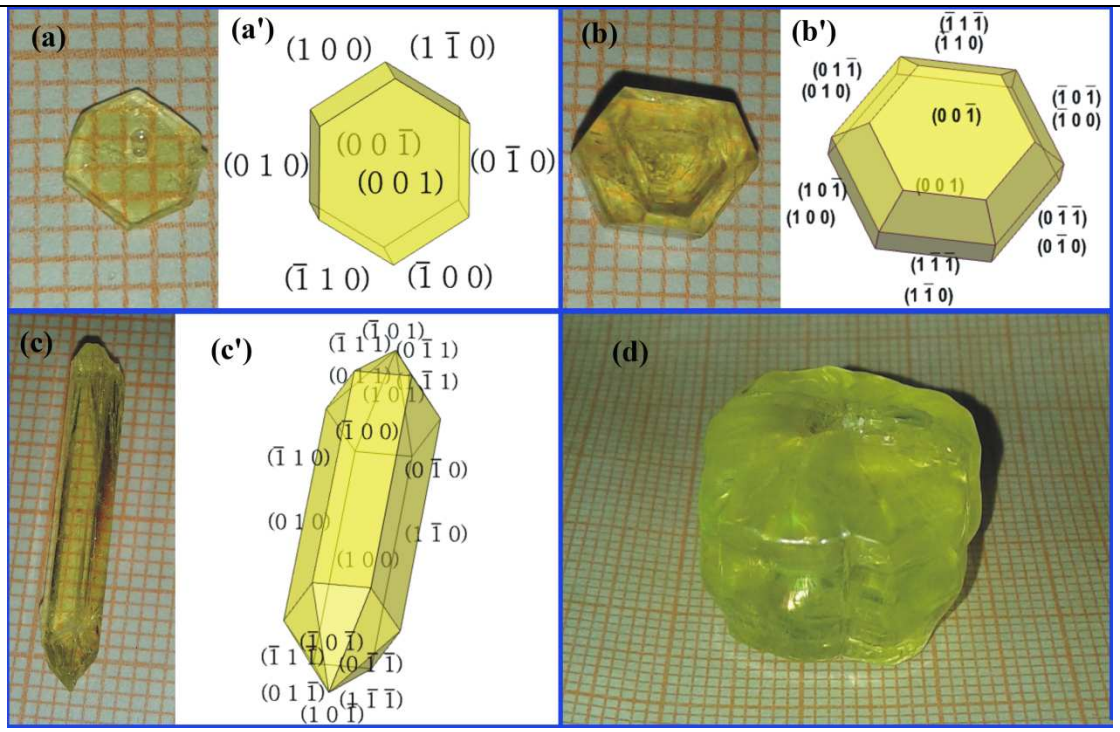

Fig. 1 (a, b,) Photographs of the slow evaporation grown benzil single crystal by using acetone as a solvent showing initial and developed morphologies. (a', b') Various faces deduced theoretically by BDFH law for the benzil crystals depicted in (a) and (b), respectively. (c) Solution grown benzil crystal in the presence of liquid crystal (5CB) as an additive showing a bipyramidal prismatic morphology. (c') Miller indexing of the various faces of crystal shown in (c). (d) Bulk benzil single crystal grown by Cz technique.

Morphological studies

According to the geometrical consideration of the crystal, BFDH law is used to solve the morphology importance (MI_{hkl}) of the planes. BFDH law states that the rate of growth of the

plane (*hkl*) is inversely proportional to the interplanar distance d_{hkl}.[30] The benzil crystal morphology as shown in Fig.1 was deduced by using WinX-morph Software.[31] The accuracy of the BFDH law was improved by considering the effect of the adjacent planes in the modified rate equation (1). Therefore, the modified BFDH law is expressed as

$$\frac{dl_{hkl}}{dt} = \frac{R_{h_1k_1l_1}\sin\gamma + R_{h_2k_2l_2}\sin\alpha - R_{hkl}\sin(\alpha+\gamma)}{\sin\alpha\sin\gamma} \qquad 1$$

Where $R_{hkl}, R_{h_1k_1l_1}, R_{h_2k_2l_2}$ are the normal growth rates of the *hkl*, $h_1k_1l_1$ and $h_2k_2l_2$ faces and its value according to BFDH law is equal to $1/d_{hkl}$, α and γ are the interfacial angles for given *hkl* plane. On the basis of above relation, the growth rates were computed with their corresponding MI and are summarized in Table 1. Computed MI directly reflects the corresponding area of crystal faces according to their weightage (Fig. 1(a', b')).

Table 1 Morphological importance of benzil crystal faces from modified BFDH law

Faces (*hkl*)	d_{hkl}(Å)	Calculated relative growth rates from BFDH law	$\frac{dl_{hkl}}{dt}$	Morphological importance
$(01\bar{1})$, (101), $(1\bar{1}\bar{1})$	1.581	0.63254	0.57549	4.677
$(\bar{1}10)$, (100), (010)	1.395	0.71684	0.82774	3.251
(001)	0.743	1.34589	2.69179	1

The presence of the additives, impurities and environmental factor changes the crystal morphology significantly.[32] The growth rate of the crystal plane must be affected in different habitat; slower growth crystal plane would appear with large MI and chance to cover the faces with low MI. In the saturated solution of the benzil in acetone, 0.5 M % LC (5CB) additive was mixed uniformly to investigate the change in crystal morphology. The nature of the solvent affects the electrostatic interactions; polar solvent decreases the π-stacking and vice-versa.[33] Self organize nature and dipole moment of the 5CB is larger than acetone therefore its presence increases the effective dipole moment of the solvent as compared with the pure acetone.[34] Moreover, it may be due to the effect of LC which changed the solvent polarity significantly therefore π-stacking associated with concerning planes are changed accordingly. There is no contribution of π-stacking along the direction of (001) plane. Therefore, the growth rate associated with this plane is high and as a result, it disappeared finally from the external crystal morphology (Fig. 1(c')).

Result and discussion

XRD analysis

Single crystal XRD analysis was carried out on the both benzil crystals grown by solution as well as Czochralski technique. Single crystal of dimension 0.5 mm x 0.5 mm x 0.5 mm was used for single crystal XRD characterization. Single crystal XRD confirmed the cell parameters, and it was observed that grown crystals belongs to the non-centrosymmetric space group (P_{31}) of trigonal lattice.[35] Table 2 summarizes the single crystal XRD data of benzil crystals grown by two different techniques and molecular structure of the title compound is shown in Fig. 2.

Table 2 Single crystal data and structure refinements of the benzil crystals grown by slow evaporation and Cz techniques.

Empirical formula	$C_{14}H_{10}O2$	
Formula mass (amu)	242.98	
Temperature	293 K	
Wavelength	0.71073 Å (Mo *K*α radiation)	
Crystal system, space group	trigonal, P_{31}	
	Solution grown	Cz grown
Cell length, a	8.4306 Å (10)	8.414 Å (18)
Cell length, b	8.4306 Å (10)	8.414 Å (18)
Cell length, c	13.6856 Å (17)	13.672 Å (4)
Cell angle, alpha	90.00°	90.00°
Cell angle, beta	90.00°	90.00°
Cell angle, gamma	120.00°	120.00°
Crystal size	0.5 x 0.5 x 0.5 mm^3	
Theta range for data collection	3.2-28.9°	3.2-29.0°
Limiting indices	$-9 \le h \le 10$, $-10 \le k \le 10$, $-17 \le l \le 17$	$-11 \le h \le 7$, $-11 \le k \le 11$, $-17 \le l \le 11$
Refinement method	Full-matrix least-squares on F^2	
Restraints/ parameters	1/146	1/146
Goodness-of-fit on F^2	0.817	0.966

$R[F^2 > 2\sigma(F^2)]$, $wR(F^2)$	0.053, 0.233	0.074, 0.195

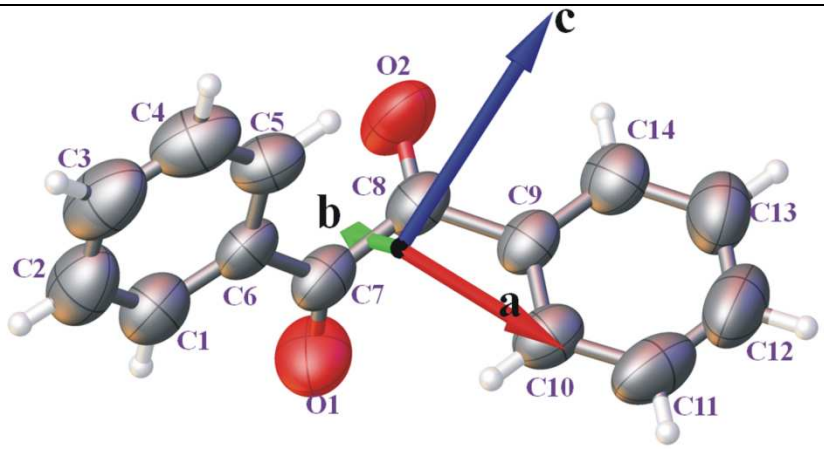

Fig. 2 X-ray crystal structure of benzil molecule (ORTEP diagrams are drawn at 50 % probability level for non-hydrogen atoms) with crystallographic numbering scheme. Crystallographic axes are denoted by **a**, **b** and **c**. Oxygen and carbon atoms are denoted by red and grey color ellipsoid balls while white color balls are for hydrogen atom.

Hirshfeld surface analysis

The notions of the modern chemistry are imbibed in a way to achieve the useful intuition in the field of crystal engineering by studying the molecular surfaces. Various models of molecular surface were reported.[36-38] Corey-Pauling-Koltumg (CPK) model was one of them in which opportune set of Van der Wall radii hard spheres was imagined at the centering positions of the atomic nuclei to generate the molecular surface.[36] To have more advanced model in this field various approaches came across in between to show better implication of this paradigm. Richard's group developed the molecular surface by using the probe sphere rolling over the CPK

surface.[37] The Van der Walls radii were varied from one crystal system to another crystal system such that it could not be fixed and, therefore, the probe radius should also be varied in different environment. Both parameters created a similar kind of problem to unify the above models for all crystal system. To overcome the above limitation, the concept of constant electron density surfaces were introduced by Bader group and here only one parameter unified the molecular surface in all crystal system by containing more than 98 % of the electronic charge in 0.002 au contour.[38] A serious drawback of the molecular surface by constant electron density concept is how to compute the wave function for macromolecules with several hundred atoms. Through the atomic fragments concept defined by Politzer and Harrris was applicable for linear molecules with absurd quantum results, therefore it was not favorable to extend this idea for non-linear molecules.[39] The above computing issue was resolved by introducing the promolecular density concept, which is equal to the total of spherically averaged electron densities for all the constituent atoms.[39] The distribution of the molecular density is according to the weight of the promolecule density at that point and defines a sharing function $w(r)$ for each atom, as

$$w_i(r) = \rho_i^{at}/\rho^{pro}(r) \text{ , where } \rho^{pro}(r) = \sum_i \rho_i^{at}(r)$$

Hirshfeld surface of a molecule in a crystal is defined by dividing the crystal electron density into molecular segments.[23]

$$w_A(r) = \sum_{i \in molecule\,A} \rho_i^{at}(r) / \sum_{i \in crystal} \rho_i^{at}(r)$$

$$= \rho_{promolecule}(r) / \rho_{procrystal}(r)$$

Hirshfeld directly relates to the space of the molecule in the crystal and generally it covers both 0.002 au electron density isosurface and hard sphere model (CPK). Hirshfeld surface is used to

understand the intermolecular interaction because it is not only connected with molecule itself but it has also contributed from nearest neighbor molecules.

The value of weight function is equal to 0.5 because at this contour one gets maximum electron density region. Intermolecular interaction was mapped on the Hirshfeld surface by choosing the distance parameter d_e (distance from the surface to the nearest nucleus outside the surface) and d_i (distance from the surface to the nearest nucleus inside the surface) and it helps to generate the two dimensional geometry by introducing fingerprint plot. To account both the inner and the outer interaction on the same surface, the term d_{norm} comes in picture which shows both interactions on the same Hirshfeld surface and is defined as.

$$d_{norm} = \frac{d_i - r_i^{vdW}}{r_i^{vdW}} + \frac{d_e - r_e^{vdW}}{r_e^{vdW}}$$

Where r_i^{vdW} and r_e^{vdW} are Van der Waals (vdW) radii of the two atoms internal and external to the molecular surface.

Different regions of the Hirshfeld surface are displayed by color code combination: red for vdW < d_{norm} and blue for vdW > d_{norm}.

The shape index (S) is defined as the local morphology of the 3-D surface and is independent of the scale.[40] It reflects the local morphology in terms of color coded information i.e. hollow (red) and bumps (blue). The shape index is expressed as

$$S = \frac{2}{\pi}\tan^{-1}\left(\frac{k_{max} + k_{min}}{k_{max} - k_{min}}\right)$$

Where, K_{max} and K_{min} is the maximum and minimum curvature of the surface.

Curvedness (C) is defined as the total curvature present within the surface[33] and is given by

$$C = \frac{2}{\pi} \ln \sqrt{\frac{k_{max}^2 + k_{min}^2}{2}}$$

The magnitude of the curvature of a surface is independent of its shape and depends on the scale in which the flat green region is separated by dark blue edges. Fig. 3(a) illustrates the molecular packing of the benzil molecule by the purple color ellipses containing the hollow red region which attributes to the close attachment with other molecules. The shape index surface pattern of the molecule is quite different in front and rear side of the molecule which corresponds to the different contact pattern with neighboring molecules. Curvedness plot shows the flat region for planer stacking arrangement which is highly dominant in the molecular surface (Fig. 3(b)).

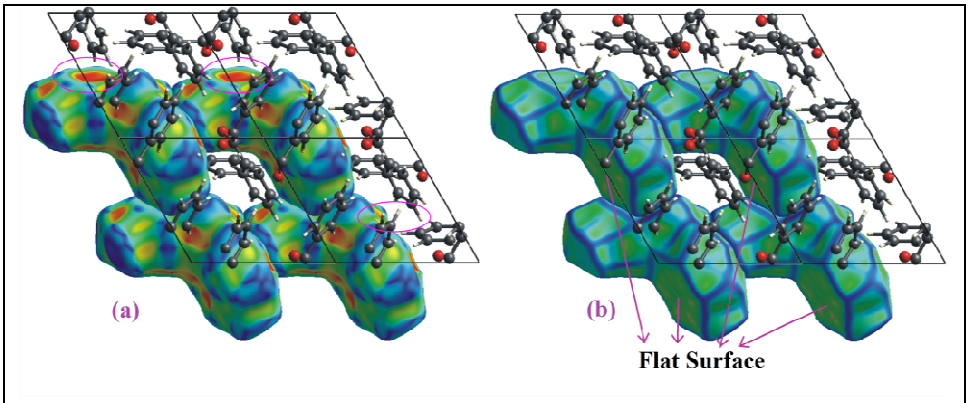

Fig. 3 (a) Hirshfeld surface of benzil molecule mapped with shape index. Self-complementary patches are represented by purple color ellipses. Hollow and bumps regions are shown by red and blue color on the shape index surfaces (b) Hirshfeld surface mapped with curvedness to identify the planer (green) and curved (blue edge) region in benzil molecule for planer stacking.

In order to understand the intermolecular interactions in Benzil crystal, we have connected it to Hirshfeld surface.

The Hirshfeld surfaces mapped with d_{norm} use a fixed color scale of negative value of -0.75 for red, positive value of 1.10 for blue and zero for white. On the molecular surface of benzil molecule as shown in Fig. 4(a), red region corresponds to the both hydrogen bond donor and acceptor equally. In order to understand the complete image of intermolecular interaction in a simplest visual manner, the 2D mapping is required to interpret all the information.[41] The fingerprint plot is a 2D plot of d_i versus d_e, which summarizes all the intermolecular interactions in benzyl molecule (Fig. 4(b)). One of the most important characteristics of the fingerprint plot is the pseudo-symmetry about the diagonal ($d_i = d_e$), which is primarily related with the close packing of the Hirshfeld surfaces. Fig. 4(c, d) shows the red region of the d_{norm} surface which attributes to the H···O ($d_e > d_i$) and O···H ($d_i > d_e$) intermolecular contacts. In the Fig. 4(e), two sharp symmetric peaks in the fingerprint plot corresponds to H···O and O···H interactions with 24% area of Hirshfeld surface. The C···H (C-H···π) contacts in benzil crystal packing is represented in the form of wings at top left and bottom right in fingerprint plot as shown in Fig. 1(f) and corresponds to the π donor ($d_e > d_i$) and acceptor ($d_i > d_e$) with 21.3% area of Hirshfeld surface.

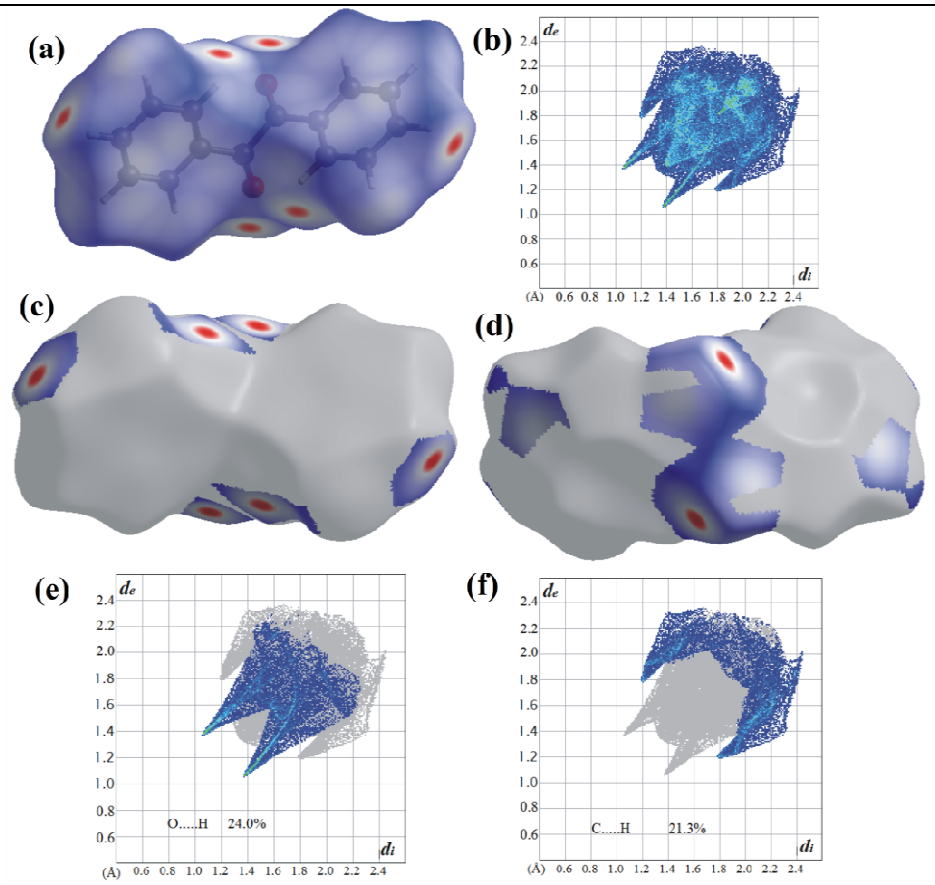

Fig. 4 (a) Hirshfeld surface mapped with d_{norm}. Red and blue colors represent the distances shorter and longer than sum of vdW radii and white color for the distances in-between for it. (b) Two-dimensional fingerprint plot for benzil molecule. (c, d) Front and back views of H···O and O···H intermolecular interactions in benzil molecule with 24% area of the 2D fingerprint plot. (e, f) Fingerprint plots of O···H and C···H. interactions with 21.3% area.

The contribution of the π···π stacking (C···C and H···H) in the benzil crystal structure was investigated by Hirsfeld surface (Fig. 5), as a red and blue triangles (labeled 1) are the characteristics of the π··· π stacking on the same region of shape index surface.[42] Fingerprint plot in Fig. 5 shows these contacts in the region pale blue color on the diagonal at around for C···C

($d_e \simeq d_i \simeq 1.8$ Å) and H···H ($d_e \simeq d_i \simeq 1.4$ Å) with combined area of 53.0 % for π···π stacking (7.7 % for C···C and 45.3 % for H···H).

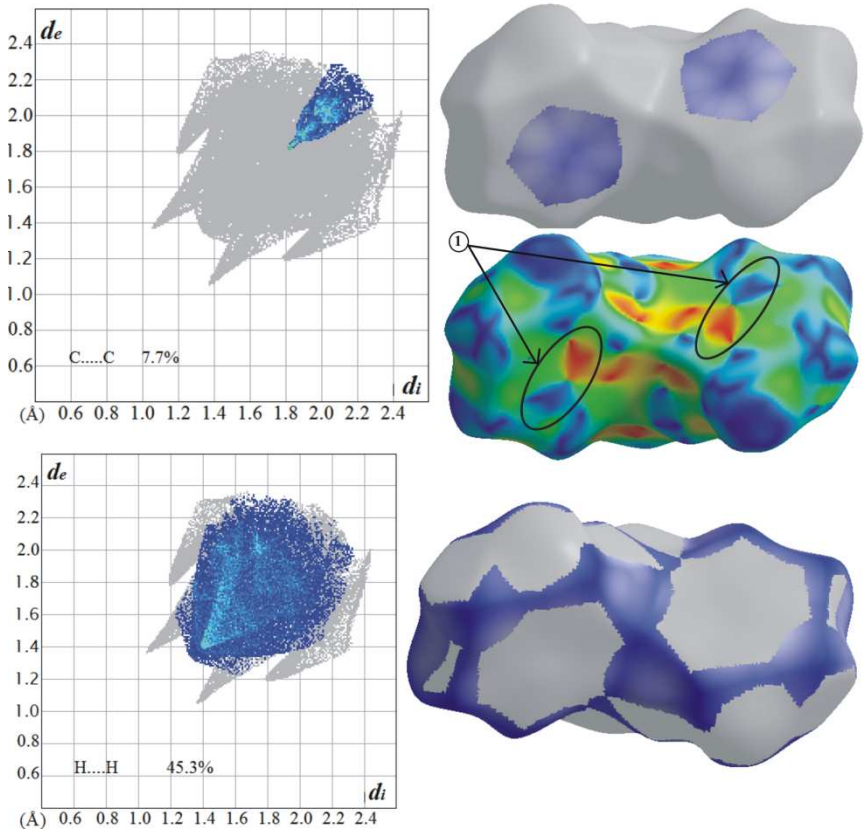

Fig. 5 Two-dimensional fingerprint plots and Hirshfeld surfaces of C···C and H···H interactions with 7.7% and 45.3% of the total intermolecular interactions area for π···π stacking of the benzil molecules. Labeled 1 region indicates π···π stacking on the shape index surface.

Optical transmission study

The optoelectronic efficiency of the NLO material is primarily decided by the transparency window in the UV-visible region. The optical transmission spectrum of the benzil crystal was recorded in the range of 200 - 1100 nm. It is observed that in the visible range Cz grown benzil

crystal has slightly better transmittance than shown by solution grown benzil crystal (Fig. 6). The low contribution of the structural grain boundaries in the Cz grown benzil crystal leads to the reduction in the scattering and multiple reflection on the incident beam.[43] The lower cut-off wavelength of solution grown crystal is 426 nm whereas Cz grown crystal is 406 nm. The lower cut-off at 440 nm in UV-Vis spectrum of benzil crystal grown by vertical dynamic gradient freeze technique in transparent furnace was reported by C. W. Lan et al.[44] Thus we have obtained a wider transparency window in the present case particularly in the Cz grown crystal. The enhancement in the optical transmission is the direct consequence of the improvement in the crystal perfection in the Cz grown crystal as compared to solution grown crystal.

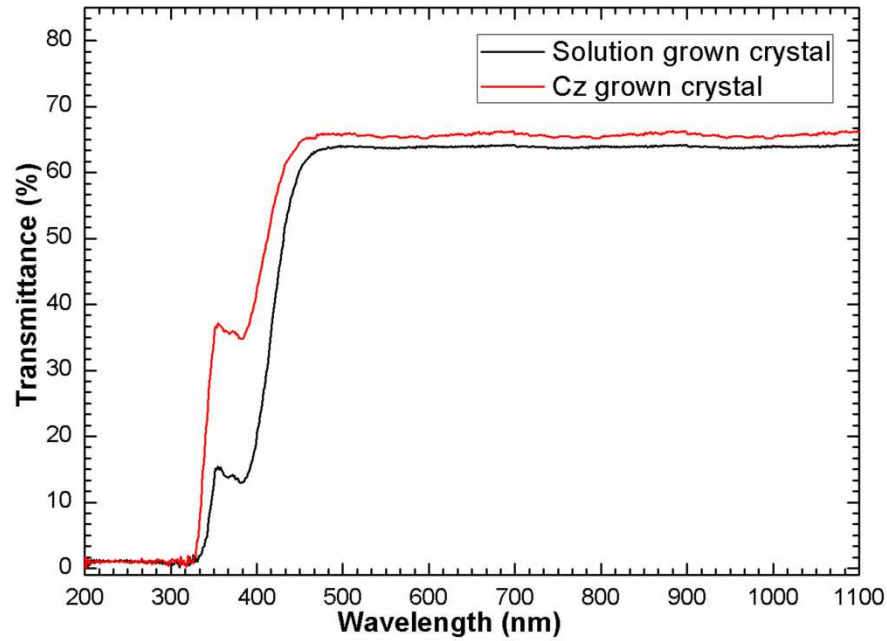

Fig. 6 UV–Vis transmission spectra of slow evaporation and Cz grown benzil crystals. A slight improvement in the transmittance and a shift in the lower cut-off value from 426 nm (solution grown crystal) to 406 nm (Cz grown crystal) was observed.

Photoluminescence

Fig. 7 illustrates the photoluminescence spectra of the Cz and solution grown benzil crystal. Both the crystals were excited at 384 nm. The broad emission spectra for both the crystals were observed at 503 nm.[45] The intensity of the PL in Cz grown crystal is higher than the solution grown crystal. The room temperature spectrum of the benzil molecule is consistent with the literature in which the emission at 505 nm is reported.[17] In the ground state benzil molecule exists in the form of skrew configuration and there is small configuration interaction between the two halves of the molecule. After excitation, the configuration of the molecule is changed from skrew to *trans*-planer system. The lone pair electrons on the carbonyl group of benzil molecule is excited from its planer structure and assigned as (n, π^*) transition. In the excited state, phenyl group of the benzil molecule exists in some possible configurations due to the rotation about central carbonyl - carbonyl bond. Moreover, Diffuseness in the PL spectra arises due to this rotational freedom of phenyl groups.

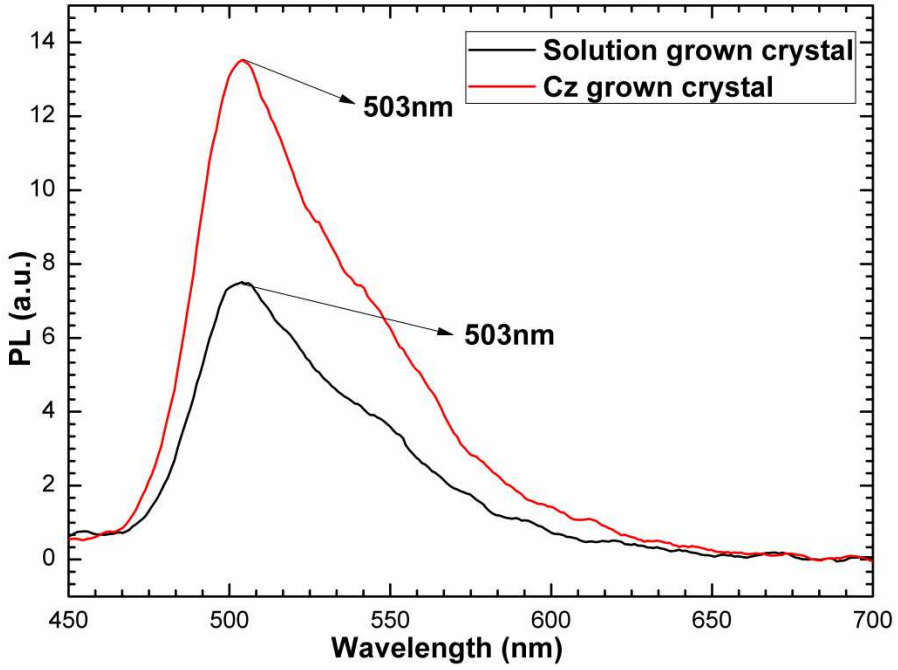

Fig. 7 Photoluminescence spectra of benzil crystals. The emission peak was found at 503 nm for both grown crystals (slow evaporation and Cz) with higher intensity in Cz grown crystal.

Piezoelectric property

Piezoelectricity is the appearance of electric potential across the crystal surface when subjected to mechanical stress. The piezoelectric charge coefficient d_{33} value has been measured along the poling direction of crystal axis. For d_{33} measurement, crystal was coated with silver paste for electrical contact and a DC poling field was applied on the crystal for 20 min across different sets of parallel crystal planes. The d_{33} values of Benzil crystal are 4, 1, 6 and 3 pC/N along the directions [100], [010], [001] and $[\bar{1}10]$. In the organic crystals, piezoelectric properties mainly

depend on the hydrogen bond and π···π stacking in molecules of the crystal.[19] In the presence of electric field, the direct polarization of the hydrogen bond is affected by the resultant of the projection of hydrogen bonds on polarization axis of the crystal. Screening effect of π···π system decreases the local field strength to polarize the hydrogen bond.[19] In the benzil crystal the contribution of the number of hydrogen bond is larger along the (001) plane and low contribution of π···π stacking along it. For these reasons, the observed piezoelectric coefficient for (001) plane is more than other planes. Due to piezoelectric property, benzil single crystal can be used for various sensor applications.

Dielectric and patch antenna analysis

The tunability of the dielectric constant in the piezoelectric material is directly used in sensor applications. The dielectric measurement of benzil crystal grown by two different techniques was characterized in the frequency range (20 Hz - 2 MHZ). The resonance peak of piezoelectric crystal depends on the dimensions of the grown crystal. A resonance phenomenon is occurred in piezoelectric crystal when the applied electric field frequency matches with its fundamental frequency.[46] Sample A represents the crystal grown by Cz technique and Sample B corresponds to the crystal grown by slow evaporation method. Dielectric constant depends on the bulk polarisability of the material. The behavior of the bulk polarisability is determined by the response of electronic, ionic, orientational and space charge in alternating electric field.[47] The defects in the material also affects the dielectric constant since the surface charges are trapped around them. The variation of the dielectric constant versus frequency with or without constant DC bias (20 V/cm) is shown in Fig. 8(a) for two different samples (A & B). The value of dielectric constant in Cz grown benzil crystal is larger due to the better crystalline perfection as

compared with the slow evaporation grown crystal. Piezoelectric crystal produces strain by the virtue of applied electric field which is correlated with its dielectric properties to tune for various applications.[48] Dielectric constant increases with applied DC voltage which can be attributed to the polarization of the material that increases with an applied electric field. The low value of dielectric constant (5.1) in benzil crystal makes it useful for thick substrate for patch antenna with better efficiency and large bandwidth.[20]

Patch antennas are popular due to many wireless applications, simplest planer design and compact size with low fabrication cost.[49] Transmission line model was used to analyze the mechanism and to calculate the dimension of patch antenna for a selected resonating frequency (12.60 GHz). The dimension parameters were calculated by the following formulas given below (1 - 4).

The patch antenna was designed at f_r = 12.6 GHz with dielectric constant 5.1 (ε_r) and thickness of the dielectric substrate as 1.02 mm (h).

At the resonant frequency f_r, the geometrical width of the patch antenna has been calculated as,

$$W = \frac{c}{2f_r}\sqrt{\frac{2}{\varepsilon_r+1}} = 6.81\text{mm} \qquad 1$$

The effective dielectric constant was calculated with respected to given h and ε_r as,

$$\varepsilon_{eff} = \frac{\varepsilon_r+1}{2} + \frac{\varepsilon_r-1}{2}\frac{1}{\sqrt{1+\frac{12h}{W}}} = 4.28 \qquad 2$$

The appropriate geometrical length was calculated from length extension (ΔL) subtrated from length of patch antenna.

$$\Delta L = 0.412 \times h \frac{(\varepsilon_{eff}+0.3)(\frac{W}{h}+0.264)}{(\varepsilon_{eff}-0.258)(\frac{W}{h}+0.8)} = 0.44 \text{ mm} \quad (3)$$

$$L = \frac{c}{2f_r\sqrt{\varepsilon_{eff}}} - 2 \times \Delta L = 4.86 \text{ mm} \quad (4)$$

Simulation of the proposed patch antenna geometry has been performed by CST Microwave Studio at 12.6 GHz operating frequency. The microstrip line (50 Ω) was used for inset feed. In the CST simulation environment, the matching of the impedance of the patch with feed line was achieved by cutting the appropriate dimensions of two slot in the patch antenna. Copper plate of thickness (1.04 mm) was used as a conducting material for patch as well as ground plane. Standard SMA connector was connected with its centre pin with patch feed line is shown in Fig. 8(b). The simulated result and experimentally measured S_{11} parameter of patch antenna are shown in Fig. 8(c) and (d), which show resonant peaks at 12.6 GHz and 11.8 GHz, respectively. Now a DC bias of 20 V/cm is applied due to which a small increase in dielectric constant (ε_r =5.16) was observed. In the sample A, the simulation pattern has been shown (Fig. 9) in which a resonant frequency of the patch antenna at 12.5 GHz was found. The frequency agility of the benzil crystal based patch antenna is Δf_r (100 MHz) and it can be improved by large DC voltage source.

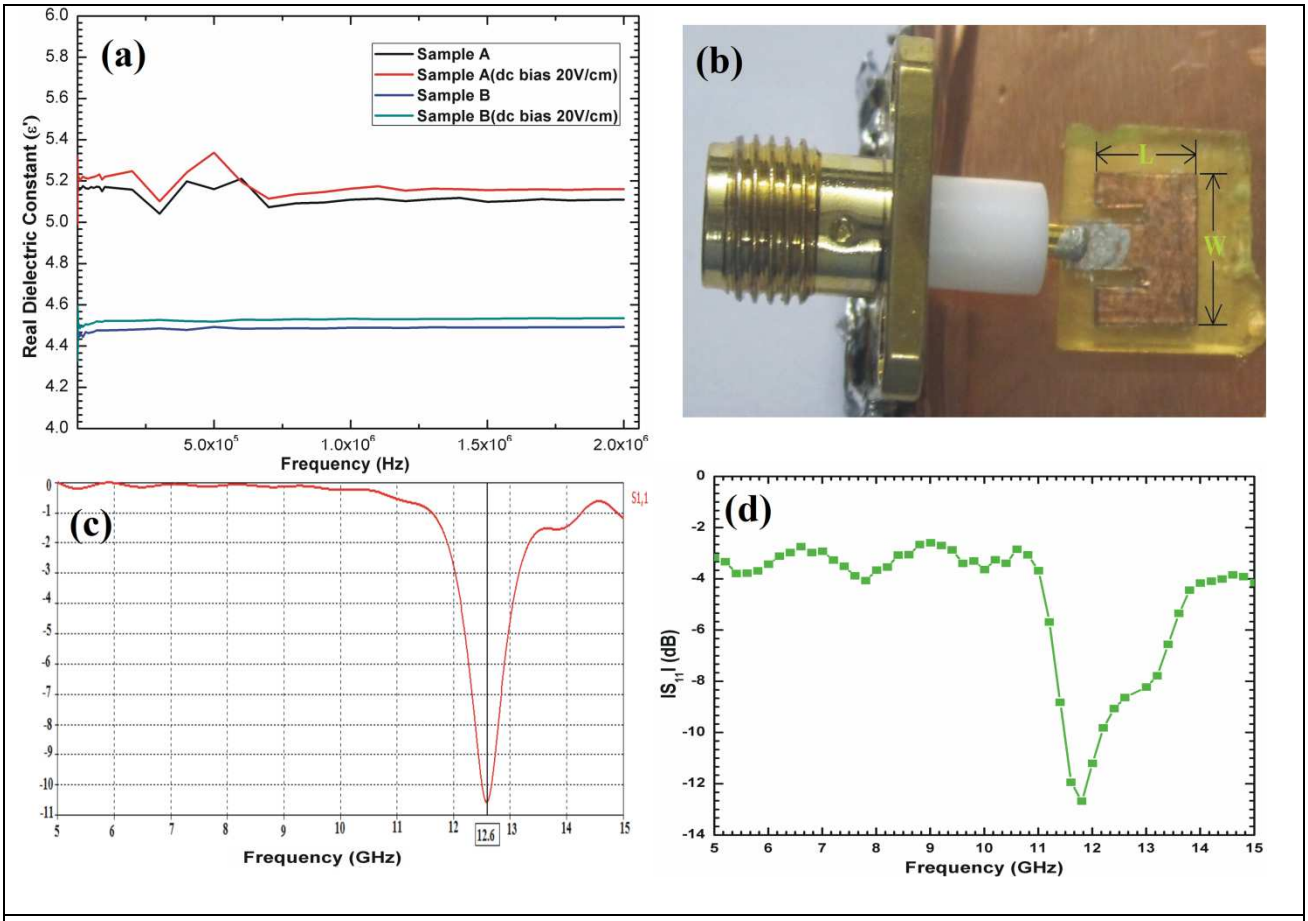

Fig. 8 (a) Plot of dilectric constant versus frequency for sample (A) and sample (B) with or without DC bias (20V/cm). (b) Photograph of fabricated patch antenna by using benzil single as a dielctric substrate (dielectric constant 'ε_r' = 5.1 and thickness 'h' = 1.02 mm). (c) Simulated S_{11} parameter versus frequency at the resonance of 12.6 GHz . (d) Measured S_{11} parameter versus frequency and observe resonace peak at 11.8 GHz.

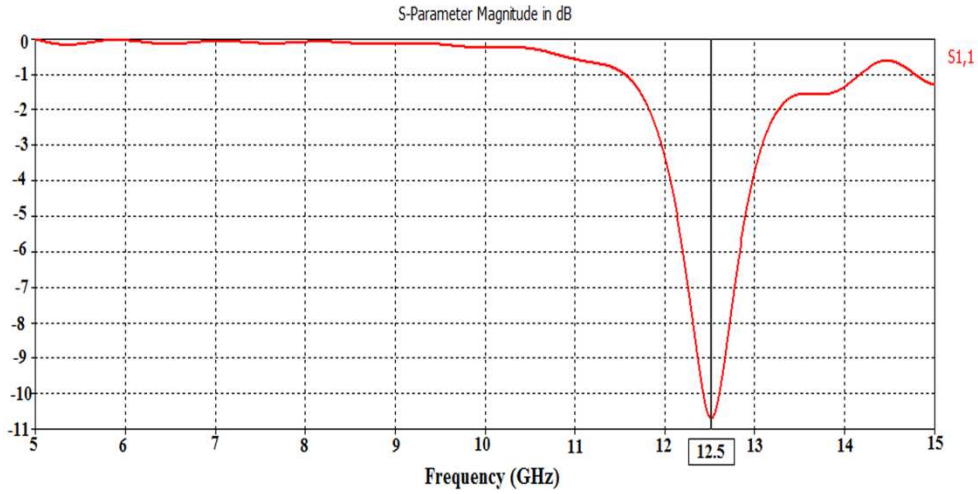

Fig. 9 Simulated S_{11} parameter with DC voltage (20 V/cm) applied and resonance peak was found at 12.5 GHz.

Microhardness analysis

Hardness of the material is determined by the resistance of a material to permanent indentation.[50] Single crystal hardness was characterized under three categories, microindentation hardness anisotropy, indentation size effect (ISE) and reverse indentation size effect (RISE).[51] Hardness of the material increases at small depths is the concept of ISE, whereas in the RISE, hardness is decreased with applied load.[52] The variation of slip system of the crystal planes in different

directions is the origin of hardness anisotropy profile. The Vicker-pyramid had been used for indentation test on the material and Vicker's hardness number (VHN) was calculated from the relation, [53]

$$H_v = KP/d^2$$

Where K is the geometrical conversion factor, P is the applied load and d is the average value of the indentation diagonals. The value of K is taken to be 1.8544, with the unit of P in kg and d in mm. The plots of Hv versus P for plane (001) of benzil crystal grown by two different techniques (Cz and slow evaporation) are shown in Fig. 10. In the case of Cz grown crystal the value of H_v is larger as compared to solution grown crystal and both the cases show the same ISE effect behavior up to 20g. After 20g the hardness number decreases due to release in energy in the form of cracks in the crystal. Initially the penetration depth of the indentor is comparable or greater than distorted zone. On further increase in the depth impression of the indentor, the variation of VHN is less prominent.

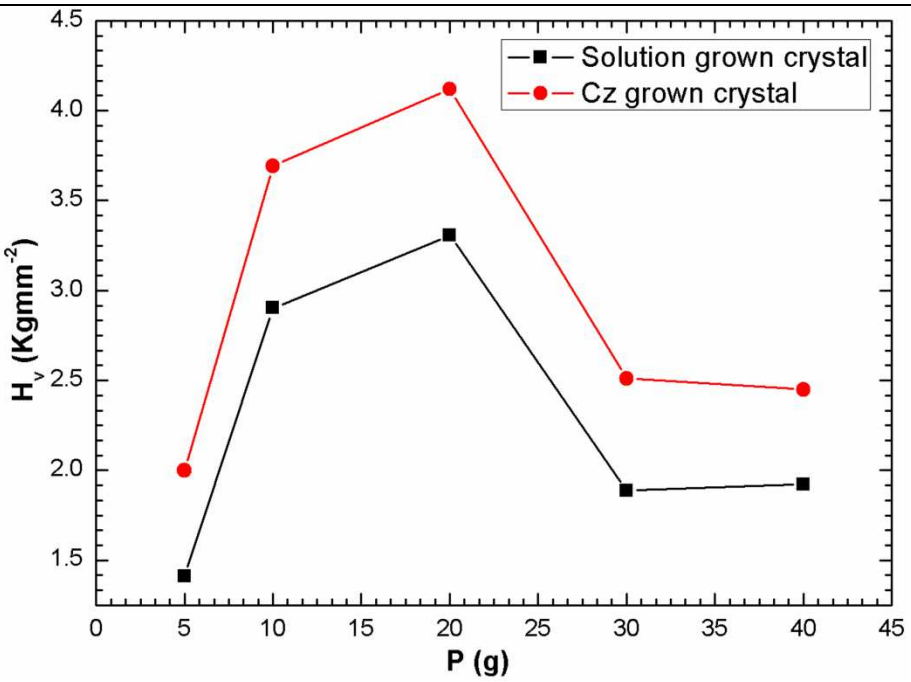

Fig. 10. Plot of the microhardness profile vs. load for (001) planes of the Cz and slow evaporation grown benzil single crystal.

The anisotropic properties of the molecular solids are equally dependent on the empty space as well as on the filled ones. The mapping of the voids in the crystalline material is constructed by isosurface (0.002 au) of procrystal electron density. Promolecular surface is used to demonstrate the surface that belongs to the molecule as well as to the empty space in the crystal.[24] Fig. 11 displays the voids surfaces of Cz and solution grown benzil single crystal. Table 3 summarizes the volumes of the voids in the both crystal (Cz & solution grown) which was computed at 0.002 au isosurface. It was concluded from the void volume of the benzil crystals for two different techniques that harness of the Cz grown crystal is larger than solution grown crystal due to the less occupied void volume as compared to the volume of solution grown crystal.

Table 3 Comparisons of different parameters of voids in the benzil crystals grown by two different techniques.

S.No	Benzil crystal	Volume/Å^3	Surface area/ Å^2	% of cell volume
1.	Cz grown (A)	111.12	415.75	13.25
2	Solution grown (B)	113.06	420.67	13.42

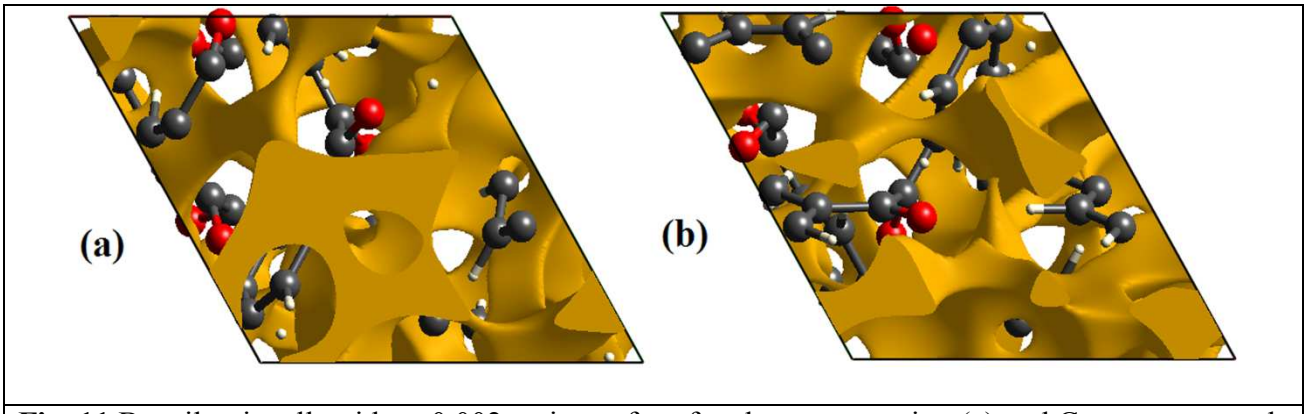

Fig. 11 Benzil unit cell voids at 0.002 au isosurface for slow evaporation (a) and Cz grown crystals (b) along crystallographic 'c' axis.

Conclusion

Transparent benzil crystals were successfully grown by Cz and slow evaporation techniques. Single crystal XRD confirmed that grown crystal has trigonal lattice with P_{31} space group. Experimentally observed morphology was confirmed by modified BDFH law. All of the intermolecular interactions present in benzil crystal were reveled from 3D Hirshfeld surfaces and 2D fingerprint plots, which are not visualized by any other convention crystal packing models.

The optical transparency and PL yield are higher in Cz grown crystal which is a direct consequence of the higher crystallinity. The piezoelectric coefficient was measured across different directions and found to be highest (6 pC/N) along the [001]. In the hardness studies, Cz grown crystal was found to be mechanically more stable as compared to that grown with the solution technique. A patch antenna based on benzil crystal was simulated for a frequency of 12.6 GHz. Desired patch antenna was fabricated using Cz grown crystal and the resonant frequency was measured as 11.8 GHz. A shift in resonant frequency of 100 MHz by applying DC voltage was also simulated. Patch antenna based on benzil crystal substrate not only used as a communication purpose but also has a potential for various sensors application.

Acknowledgements

We are thankful for the financial support received in the DST project (Sanction No SR/S2/CMP-0068/2010). Harsh Yadav is thankful to UGC for Meritorious Scholarship.

References

1 R. T. Bailey, F. R. Cruickshank, P. Pavlides, D. Pugh and J. N.Sherwood, *J. Phys. D: Appl. Phys.*, 1991, **24**, 135-145.

2 G. R. Kumar and S. G. Raj, *Adv. Mater. Sci. Eng.*, 2009, **2009**, 1-40.

3 D. S. Chemla and J. Zyss, *Nonlinear optical properties of organic molecules and crystals*, Academic Press, Orlando, FL (USA), 1987, Vol. 4, Ch. vii, pp 182-184.

4 N. Goel, N. Sinha and B. Kumar, *Mater. Res. Bull.*, 2013**, 48**, 1632-1636**.**

5 B. D. Hatton, K. Landskron, W. J. Hunks, M. R. Bennett, D. Shukaris, D. D. Perovic and G. A. Ozin, *Mater. Today*, 2006, **9**, 22-31.

6 J. Petzelt, Yu. G. Gonoharov, G. V. Kozlov, A. A. Volkov, B. Wyncke and F. Brehat, *Czech. J. Phys.*, 1984, ***B34***, 887-890.

7 T. Suthan, P. V. Dhanaraj, N. P. Rajesh, C. K. Mahadevan and G. Bhagavannarayana, *CrystEngComm*, 2011, **13**, 4018-4024.

8 M. Rajalakshmi, T.S. Shyju, R. Indirajith and R. Gopalakrishnan, *Spectrochimica Acta Part A*, 2012, **86**, 27– 32.

9 K. Sankaranarayanan and P. Ramasamy*, J. Cryst. Growth*, 1998, **193**, 252-256.

10 M. V. Shankar and K. B. R. Varma, *Bull. Mater. Sci.,* 1996, **19**, 791-798.

11 A. Stanculescu, S. Antohe, H. V. Alexandru, L. Tugulea, F. Stanculescu and M. Socol, *Synt. Met.,* 2004, **147**, 215–220.

12 Th. Scheffen-Lauenroth, H. Klapper and R. A. Beckeri, *J. Cryst. Growth*, 1981, **55**, 557-570.

13 K. Katoh and N. Kato, *J. Cryst. Growth*, 1985, **73**, 203–210.

14 M. D. Aggarwal, W. S. Wang and M. Tambwe, *J. Cryst. Growth*, 1993, **128**, 891–896.

15 A. Yoshihara, E. R. Bernstein, and J. C. Raich, *J. Chem. Phys.*, 1982, **77**, 2768-2778.

16 S. C. Bera, R. Mukherjee, and M. Chowdhury, *J. Chem. Phys.*, 1969, **51**, 754-761.

17 B. Ma, L. F. Vieira Ferreira, and P. Coppens, *Org. Lett.*, 2004, **6**, 1087–1090.

18 T. Kanagasekaran, P. Mythili, P. Srinivasan, Ahmad Y. Nooraldeen, P. K. Palanisamy, and R. Gopalakrishnan, *Cryst. Growth Des.*, 2008, **8**, 2335-2339.

19 K. A. Werling, G. R. Hutchison and D. S. Lambrecht, *J. Phys. Chem. Lett.*, 2013, **4**, 1365−1370.

20 C. A. Balanis, *Antenna theory*, John Wiley & Sons, Inc., 2007; C. 14, pp 722-752.

21 K. Sangwal, *Additives and Crystallization Processes: From Fundamentals to Applications,* John Wiley & Sons, Ltd, 2007, Ch. 1, pp 8-9.

22 J. Prywer, *J. Cryst. Growth*. 2004, **270**, 699–710.

23 M. A. Spackman and D. Jayatilaka, *CrystEngComm*, 2009, **11**, 19-32.

24 M. J. Turner, J. J. McKinnon, D. Jayatilaka and M. A. Spackman, *CrystEngComm*, 2011, **13**, 1804-1813.

25 C. K. Ghosh and S. K. Parui, *IJEEI*, 2010**, 2,** 102-112.

26 I. Mohammad, V. Gowda, H. Zhai and H. Huang, *Meas. Sci. Technol.*, 2012, **23**, 015102.

27 J. T. Song, I. H. Cho and Y. H. Kim, *Jpn. J. Appl. Phys.*, 2001**, 40***,* 515-517.

28 J. C. Myers, B. S. Strachan, X. Yang and P. Chahal, *2013 IEEE 63rd Electron. Components Technol. Conf.* 2013, 1662–1666.

29 S. K. Wolff, D. J. Grimwood, J. J. McKinnon, M. J. Turner, D. Jayatilaka and M. A. Spackman, *CrystalExplorer 3.1,* University of Western Australia, 2012.

30 M. A. Deij, J. van Eupen, H. Meekes, P. Verwer, P. Bennema and E. Vlieg, *Int. J. Pharm.*, 2008, **353**, 113–23.

31 W. K. Aminsky, *J. Appl. Cryst*., 2005, **38**, 566-567.

32 C. Schmidt and J. Ulrich, *J. Cryst. Growth*, 2012, **353**, 168–173.

33 F. J. Punzo, *Mol. Struct.*, 2013, **1032**, 147–154.

34 I. Dierking, G. Scalia, P. Morales and D. LeClere, *Adv. Mater.*, 2004, **16**, 865–869.

35 C. J. Brown and R. Sadanaga, *Acta Cryst*., 1965, **18**, 158-164.

36 F. R. N. Gurd, *Biochem. Educ.*, 1974, **2**, 27-29.

37 A. S. Mitchell and M. A. Spackman, *J. Comput. Chem.*, 2000, **21**, 933-942.

38 R. F. W. Bader, W. H. Henneker and P. E. Cade, *J. Chem. Phys.*, 1967, **46**, 3341-3363.

39 F. L. Hirshfeld, *Theor. Chim. Acta*, 1977, **44**, 129–138.

40 A. Roberts, *First Break*, 2001, **19**, 85–100.

41 M. A. Spackman and J. J. McKinnon, *CrystEngComm*, 2002, **4**, 378-392.

42 J. J. McKinnon, M. A. Spackman and A. S. Mitchell, *Acta Crystallogr. Sect. B.*, 2004, **60**, 627–668.

43 S. K. Kushwaha, N. Vijayan, K. K. Maurya, A. Kumar, and B. Kumar, *J. Appl. Cryst.,* 2011, **44**, 839–845.

44 C. W. Lan and C. R. Song, J. Cryst. Growth, 1997, **180**, 127–135.

45 D. J. Morantz and A. J. C. Wright, *J. Chem. Phys.*, 1971, **54**, 692-697.

46 Z. Wu and K. Xi, *Ultrasonics*, 2014, **54**, 1318–1322.

47 K. C. Kao, *Dielectric Phenomenain Solids*, Elsevier Academic Press, San Diego, 2004, Ch. 2, pp 54-79.

48 H. Il. Kang and J. T. Song, *J. Korean Phys. Soc.*, 2008, **53**, 826-830.

49 H. Il. Kang, J. T. Kim and J. T. Song, *Curr. Appl. Phys.*, 2010, **10**, 642–645.

50 J. J. Gilman, *Chemistry and Physics of Mechanical Hardness*; John Wiley & Sons: New Jersey, 2009, ch. 1, pp 1-9.

51 O. Sahin, O. Uzun, U. Kolemen and N. Ucar, *Mater. Charact.*, 2007, **58**, 197–204.

52 G. M. Pharr, E. G. Herbert and Y. Gao, *Annu. Rev. Mater. Res.*, 2010, **40**, 271–292.

53 K. Sangwal and A. Klos, *Cryst. Res. Technol.*, 2005, **40**, 429–438.

Table of contents graphic

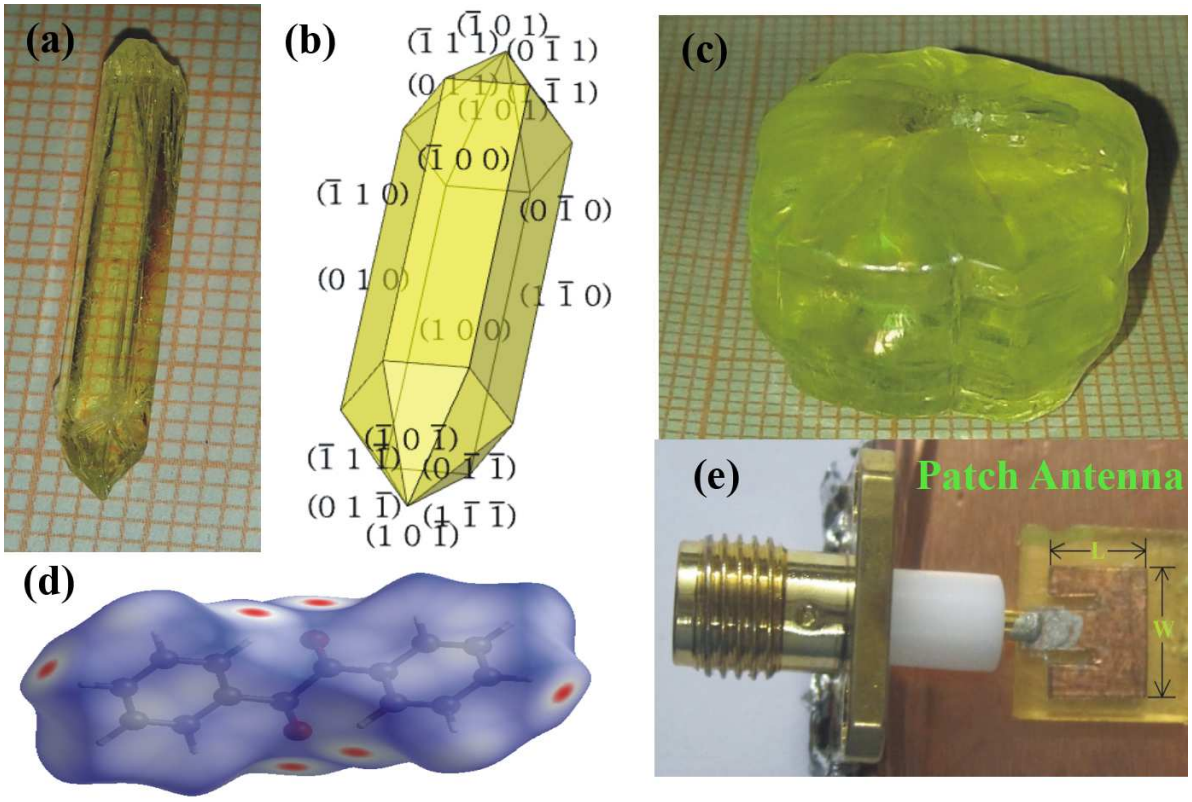

Solution and Cz grown benzil crystals (a,c) with indexed planes (b), Hirshfeld surfaces (d) and fabricated patch antenna (e).